Supplementary Information (SI) for Journal of Materials Chemistry C. This journal is ©The Royal Society of Chemistry 2025

In-situ Preparation of High-Performance Flexible Copper Halide Scintillation Films for X-ray imaging

Xianming Cai, [a] Xinxin Miao, [a] Muhammad Bilal, [a] Congxiao Wu, [b] Ruoyu Li, [a] Ahmed Uddin, [a] Jing Li, [a] Jun Pan*[a]

a College of Materials Science and Engineering, Science and Education Integration College of Energy and Carbon Neutralization, Zhejiang University of Technology,

Hangzhou 310014, China

E-mail: panjun0123@zjut.edu.cn

b College of Materials Science and Engineering, Nanjing University of Science and Technology,

Nanjing 210094, China

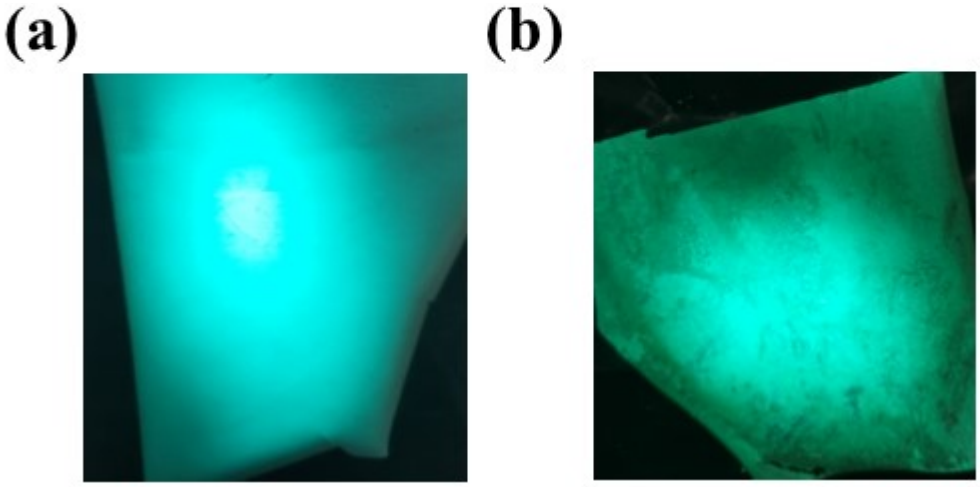

Fig. S1. Photographs of films prepared (a) with and (b) without Tween 80.

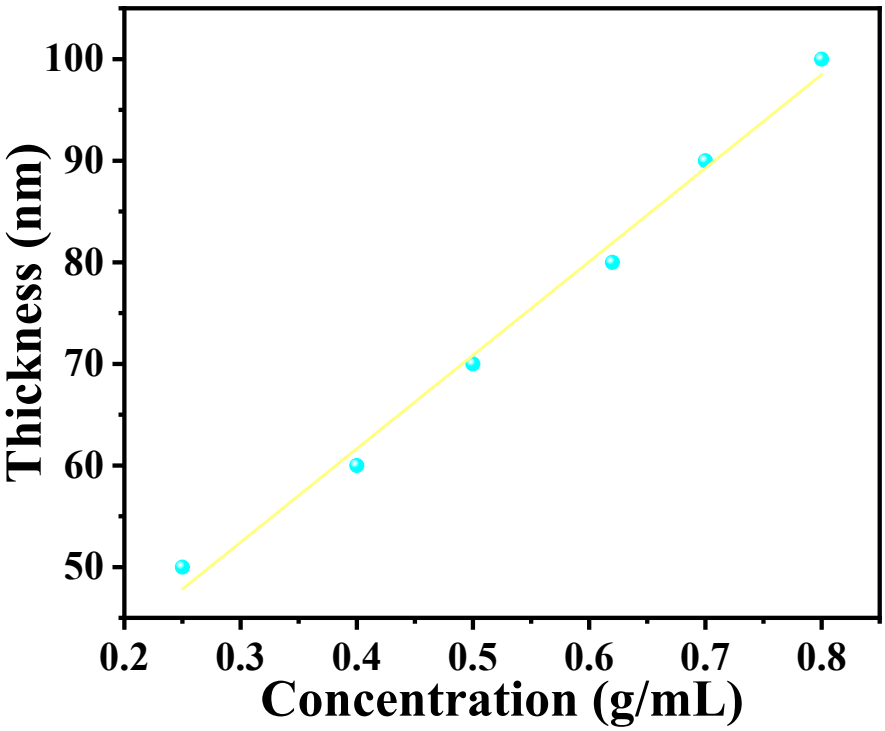

Fig. S2. The relationship between film thickness and solution concentration of $(C_{19}H_{18}P)_2CuI_3$@PMMA.

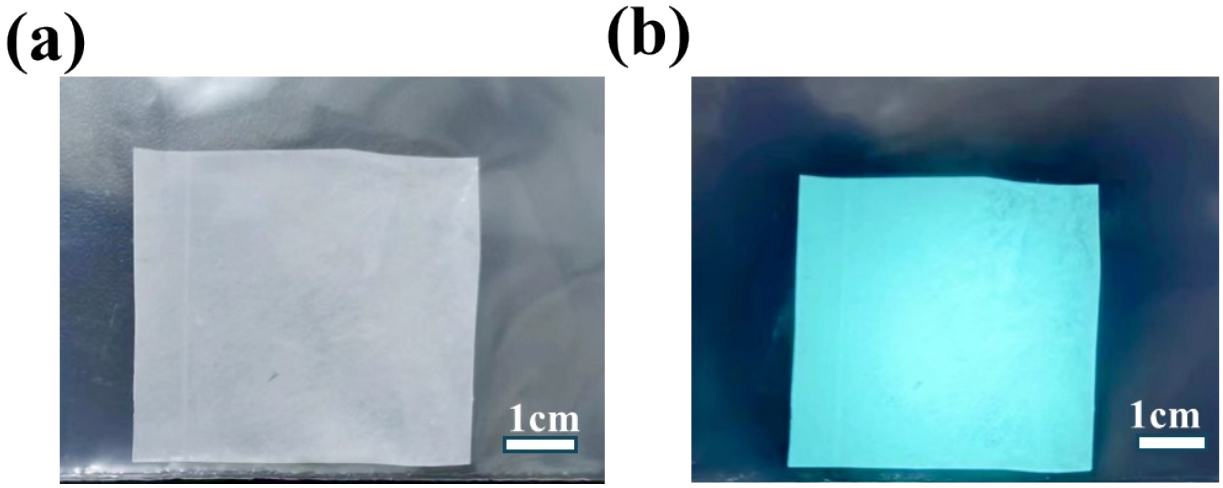

Fig. S3. Photographs of the in-situ grown $(C_{19}H_{18}P)_2CuI_3$@PMMA film: (a) under ambient light and (b) under 365 nm irradiation.

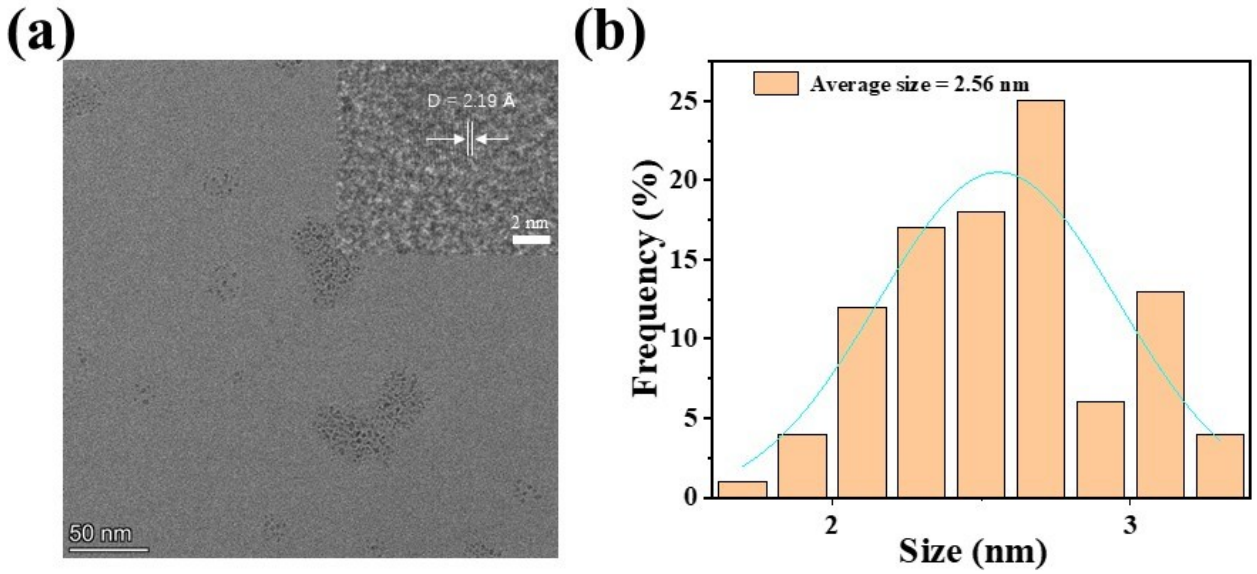

Fig. S4. (a) TEM image of the diluted precursor solution (mixture of CuI, $C_{19}H_{18}IP$, H_3PO_2 and PMMA in DMF), the inset shows the corresponding high-magnification TEM image with an interplanar distance of 2.19 Å. (b) Size distribution of $(C_{19}H_{18}P)_2CuI_3$ in PMMA matrix, the average size was 2.56 nm.

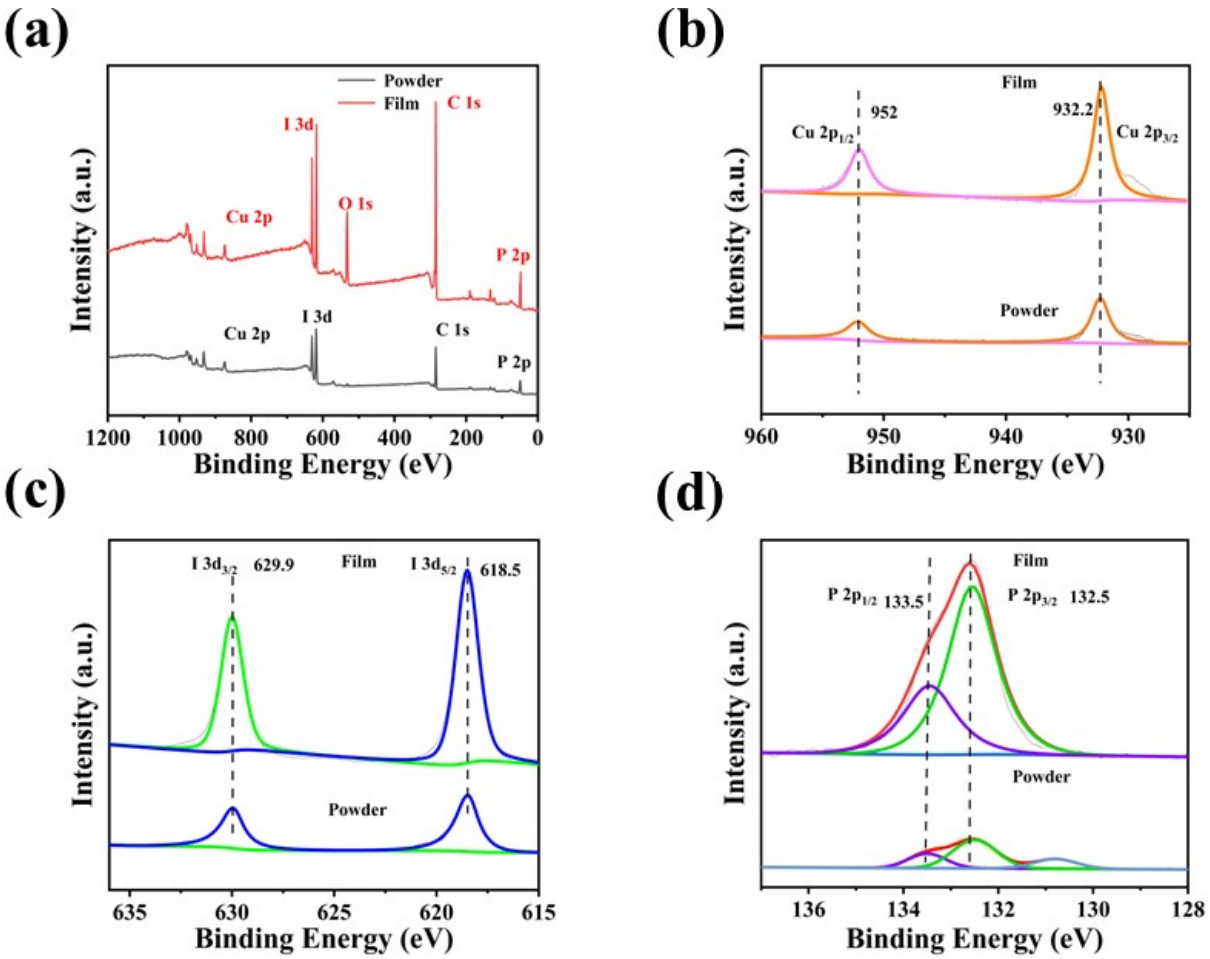

Fig. S5. XPS spectra of $(C_{19}H_{18}P)_2CuI_3$ and $(C_{19}H_{18}P)_2CuI_3$@PMMA film, peaks at 932.2 eV and 952 eV corresponding to Cu $2p_{3/2}$ and Cu $2p_{1/2}$ orbits; peaks at 618.5 eV and 629.9 eV corresponding to I $3d_{5/2}$ and I $3d_{3/2}$ orbits; peaks at 132.5 eV and 133.5 eV corresponding to P $2p_{3/2}$ and P $2p_{1/2}$ orbits (all the peak positions were corrected according to C1s orbit located at 248.8 eV).

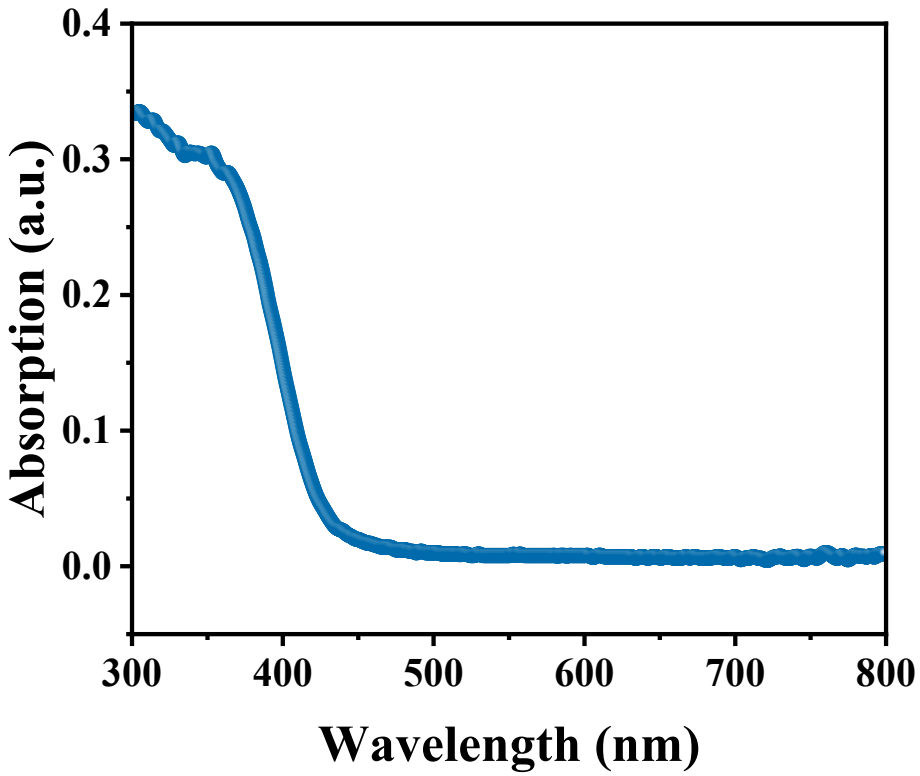

Fig. S6. UV absorption spectrum of $(C_{19}H_{18}P)_2CuI_3$@PMMA film.

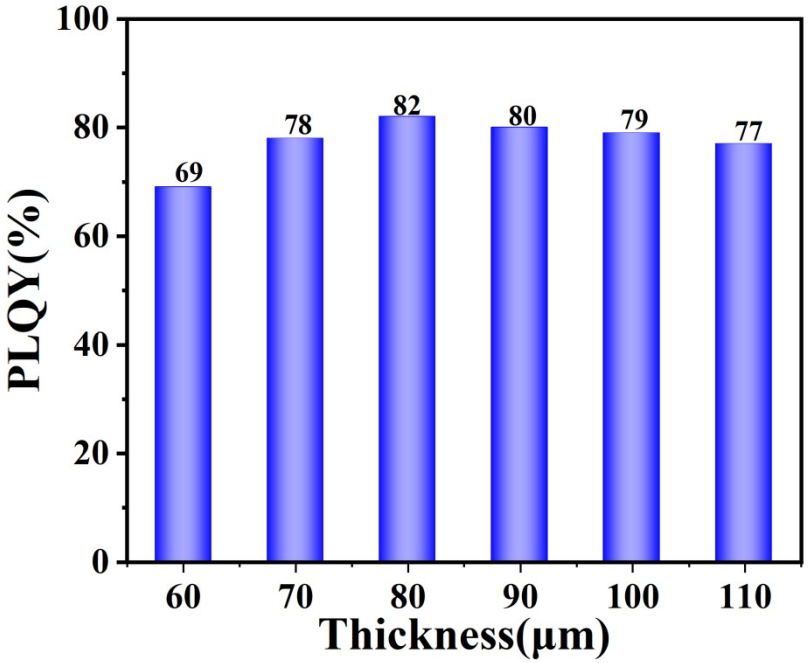

Fig. S7. PLQY of $(C_{19}H_{18}P)_2CuI_3$@PMMA films with different thicknesses.

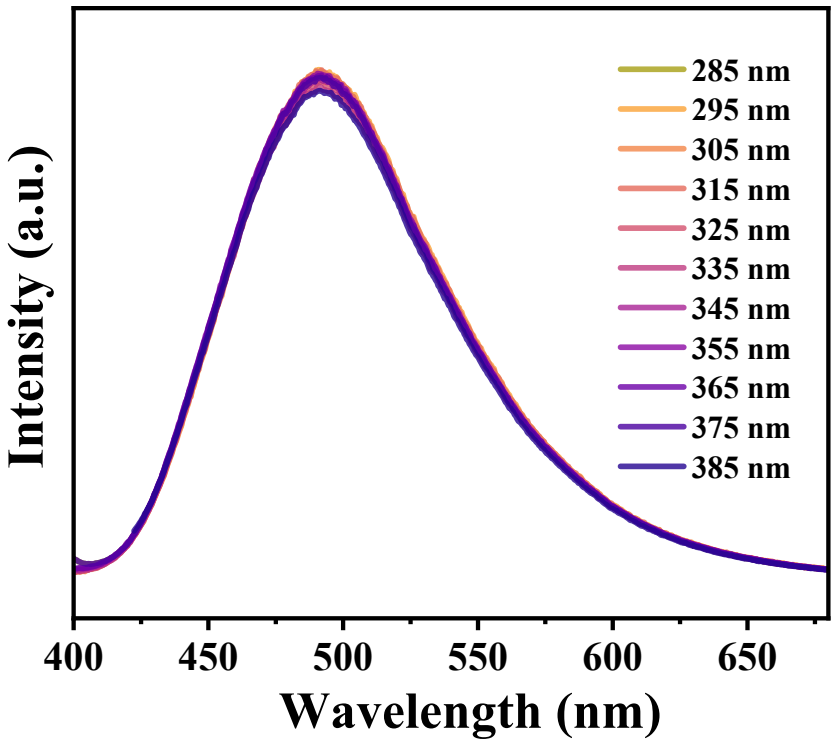

Fig. S8. PL intensity of $(C_{19}H_{18}P)_2CuI_3$@PMMA film under different excitation wavelengths from 285 nm to 385 nm.

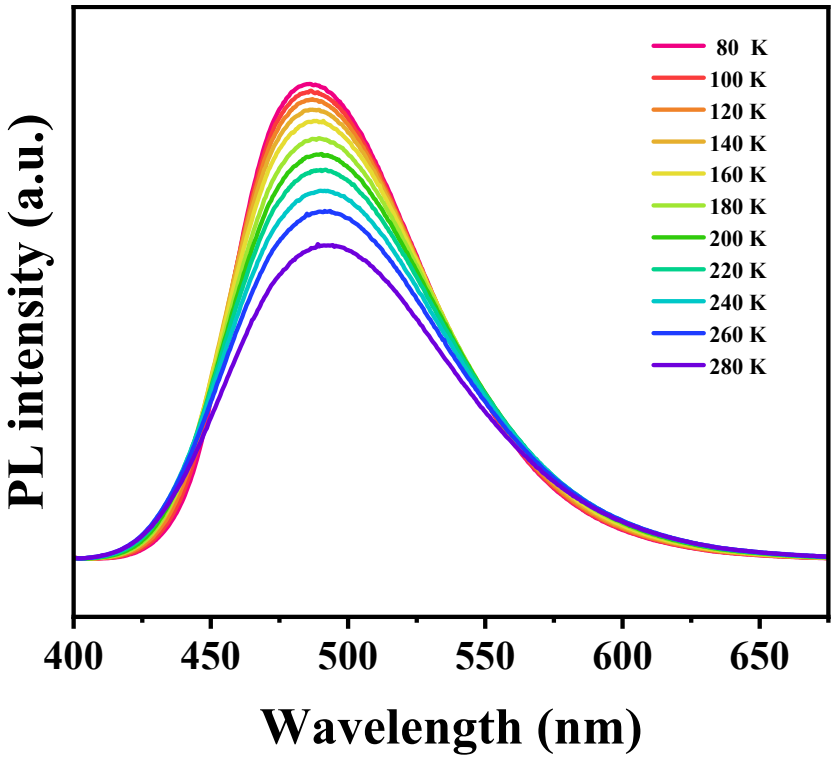

Fig. S9. Temperature-dependent PL spectra of $(C_{19}H_{18}P)_2CuI_3$@PMMA film in the range of 80–280 K.

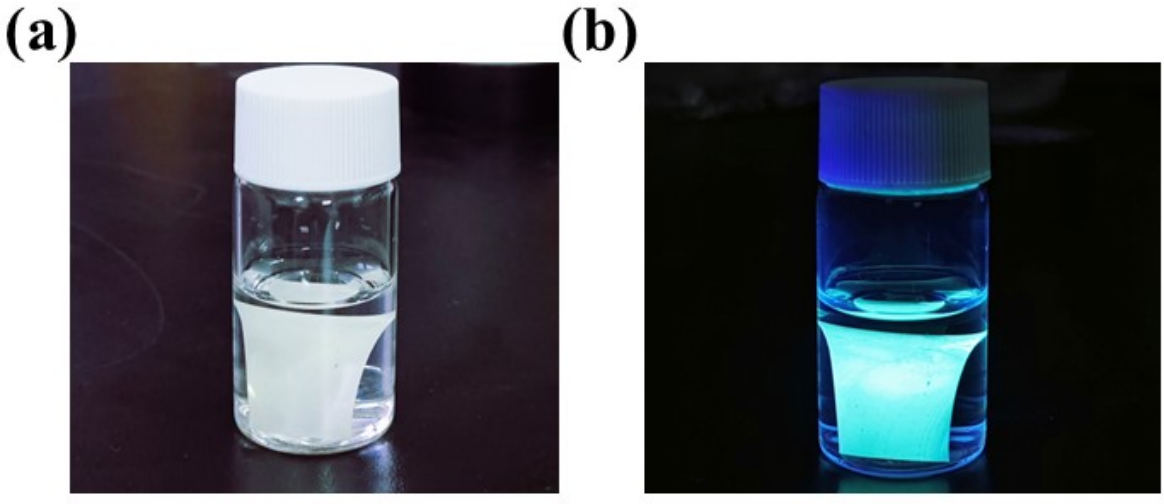

Fig. S10. Photos of the $(C_{19}H_{18}P)_2CuI_3$@PMMA film soaked in water: (a) under natural light and (b) 365 nm ultraviolet light.

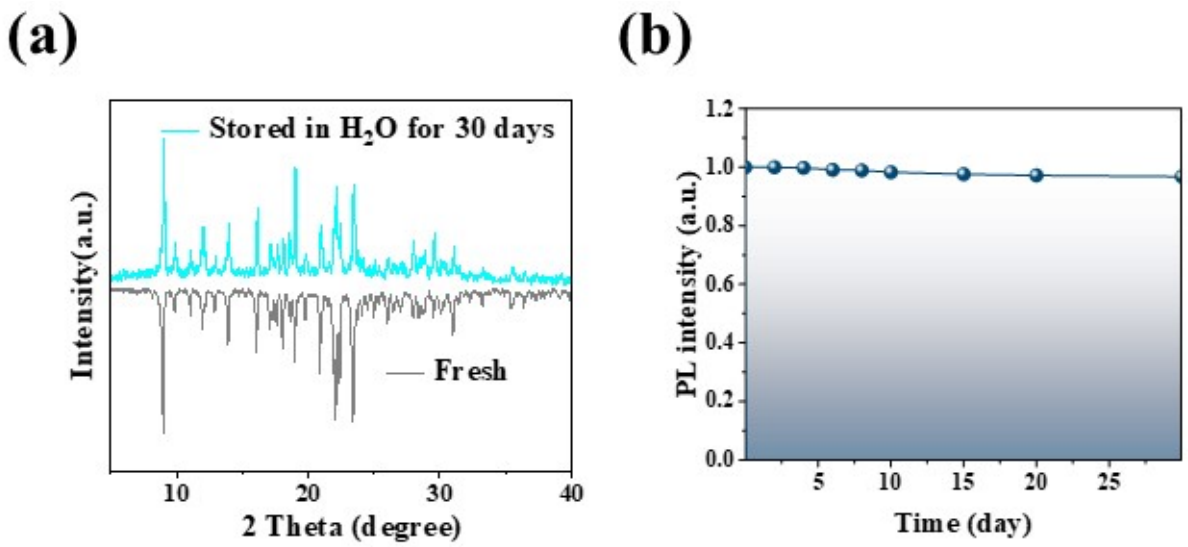

Fig. S11. (a) XRD patterns of freshly grown $(C_{19}H_{18}P)_2CuI_3$@PMMA film and after soaked in water for 30 days. (b)Variation in PL emission intensity of $(C_{19}H_{18}P)_2CuI_3$@PMMA film after being soaked in water for 30 days.

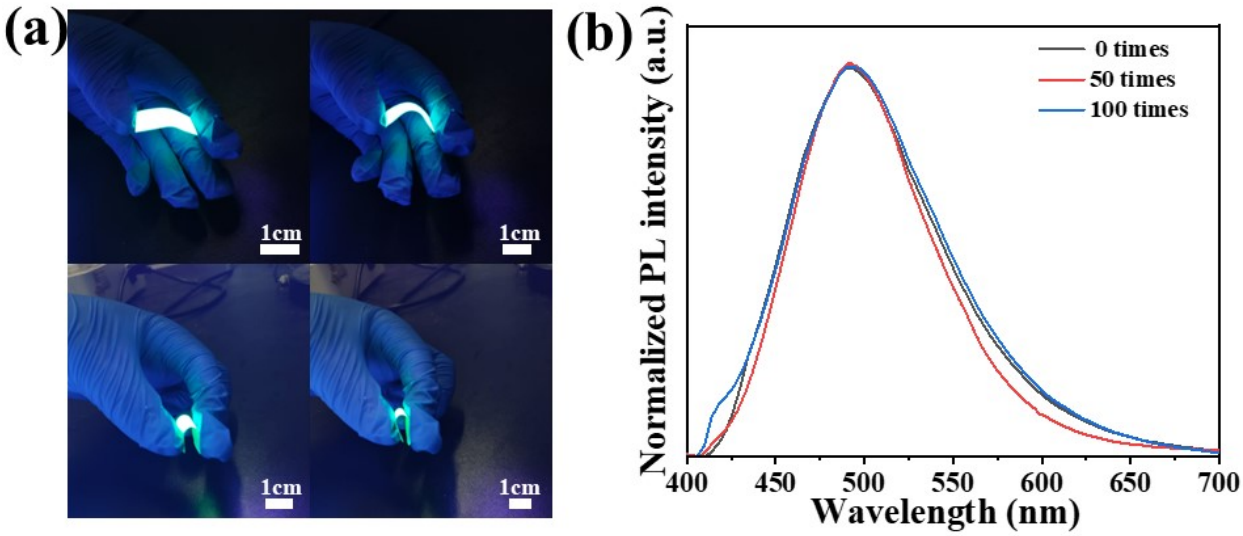

Fig. S12. (a) Photographs of $(C_{19}H_{18}P)_2CuI_3$@PMMA scintillation film at different bending states under UV 365 nm. (b) Normalized PL spectra of $(C_{19}H_{18}P)_2CuI_3$@PMMA scintillation film at different numbers of bending.

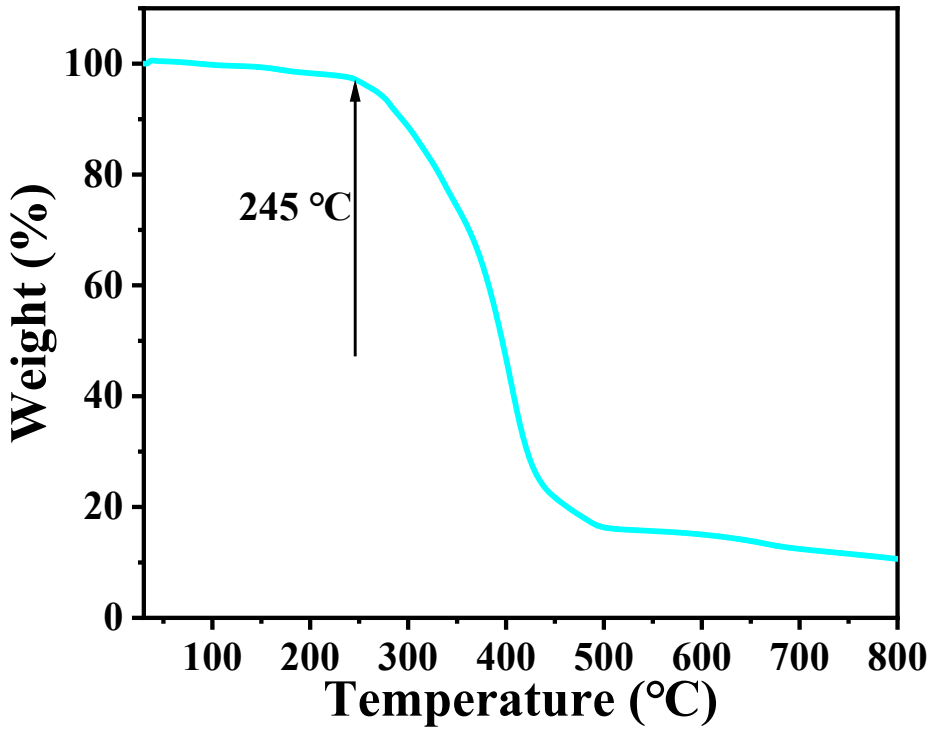

Fig. S13. Thermogravimetric curve of the $(C_{19}H_{18}P)_2CuI_3$@PMMA film.

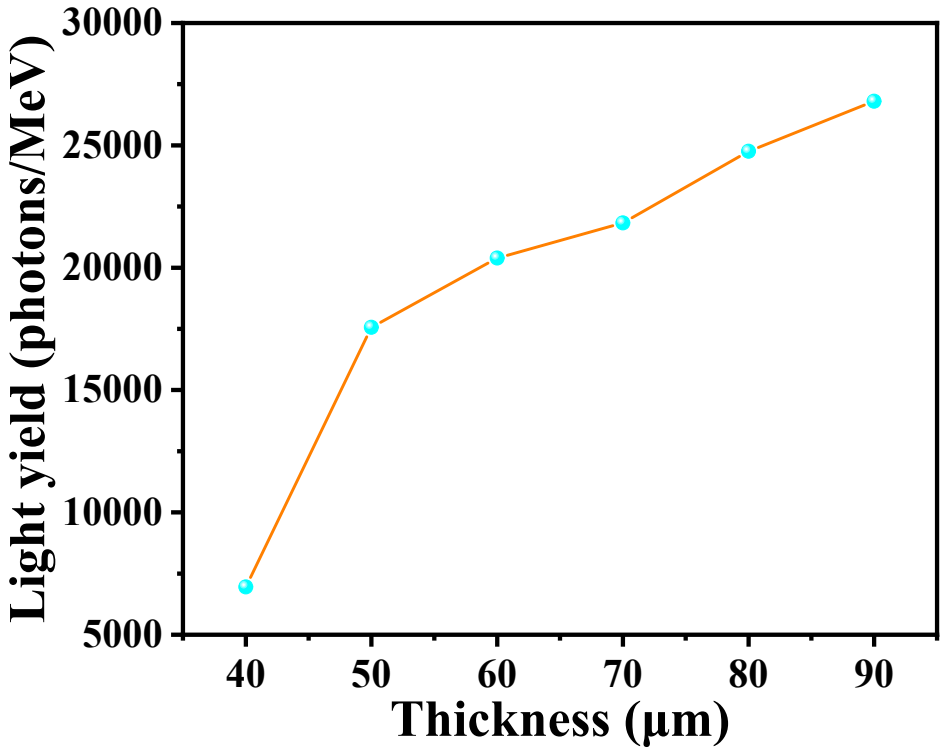

Fig. S14. Relationship between light yield and scintillator film thickness of $(C_{19}H_{18}P)_2CuI_3$@PMMA.

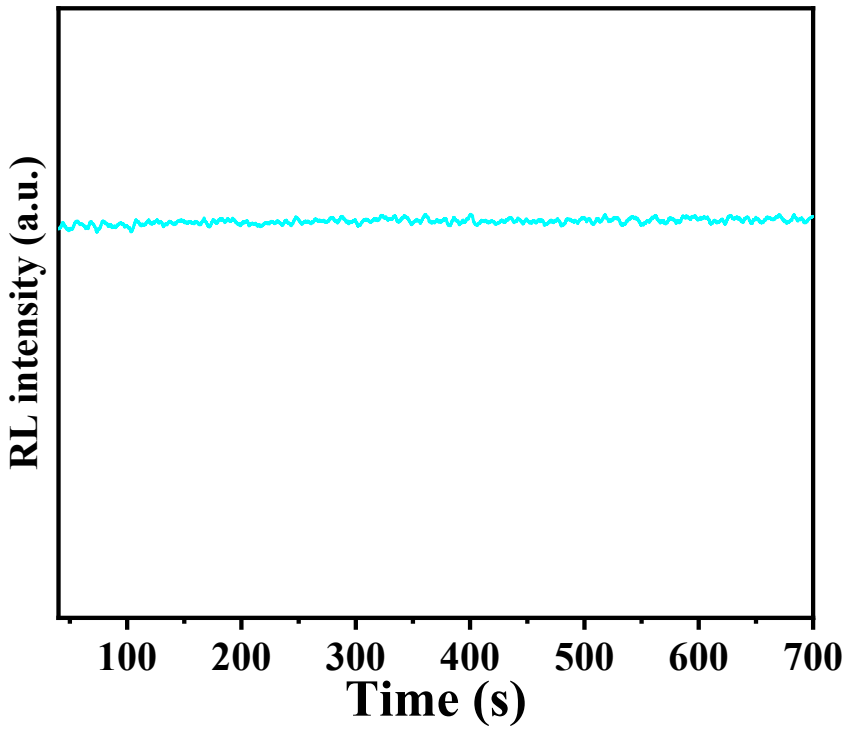

Fig. S15. Changes in RL intensity of $(C_{19}H_{18}P)_2CuI_3$@PMMA scintillator film under 10 min continuous X-ray irradiation at a dose rate of 1.221 mGy s^{-1}.